Fiber Fault PON Monitoring Using Optical Coding: Effects of Customer Geographic Distribution

Mohammad M. Rad, *Member, IEEE,* Habib A. Fathallah, *Member, IEEE,* and Leslie A. Rusch, *Fellow, IEEE*

***Abstract*—We analyze the performance of fiber fault monitoring of a PON using a centralized, passive optical coding (OC) system. We develop an expression for the detected monitoring signal, study its statistics, and contrast our OC monitoring system with standard optical code division multiplexing (OCDM) data communication. We derive a new closed form lower bound expression for the interference probability, and use this to find the signal-to-interference ratio (SIR). A service provider cannot control the physical layout of homes in a coverage area; measuring performance for one network layout would be insufficient to test our proposed monitoring system. Client geographic distribution has a significant impact on the SIR. We consider five different PON geographical distributions and study their effect on OC monitoring performance. Our results show that SIR is sufficient to successfully monitor the network. In addition, we find that the uniform radial (UR) distribution, an analytically tractable distribution, gives good performance estimation and can therefore be a useful tool in characterizing performance in terms of both SIR and signal-to-noise ratio (SNR).**

***Index Terms*—Monitoring, optical coding (OC), OCDMA, signal-to-interference ratio (SIR), PON.**

I. Introduction

As the capacity of passive optical networks (PONs) increases, allowing hundreds of clients to share the same infrastructure, the importance of performance monitoring increases [1-7]. Some service providers report that more than 80% of installed PON failures occurs within the first/last mile, i.e., within the distribution/drop segments of the network. Notwithstanding that, fiber-to-the-home (FTTH) managers still lack an efficient technology appropriate for the link quality monitoring of a PON (even the 1:32 BPON standard, ITU G.983) [6] [1]. In this paper, we focus on monitoring the link status of the PON (detecting fiber cuts or severe impairments), rather than estimating data signal quality.

It is known that optical-time-domain reflectometry (OTDR) is efficient for testing optical devices and monitoring point-to-point (PTP) networks; however, OTDR is not effective for point-to-multipoint (PMP) networks like FTTH-PONs [6,7]. In PMP networks the OTDR trace at the central office (CO) is a linear sum of the backscattered and reflected powers from all the network branches. It is difficult for the CO network manager to distinguish the events in one branch from those in others. The most important one is the difficulty to identify a specific broken branch in the PON tree architecture.

Both centralized and distributed approaches have been proposed for monitoring the fiber link status of a PON. Centralized (from the CO) approaches allow the CO to remotely acquire complete, live network information without requiring the collaboration of customers or their optical network terminals (ONTs), as does traditional OTDR in PTP networks. Distributed strategies place active modules inside the ONTs that measure performance and report to the CO. These modules are simplified, miniaturized OTDRs that periodically evaluate the uplink for specific distribution-drop fiber (DDF) segments. The distributed approach is a good tool to identify fiber link degradation; however, it is ineffective when there is an interruption in the DDF, e.g., a fiber cut. For instance, a client relocating the ONT could be misinterpreted as a fiber break.

Few centralized techniques have been previously proposed for in-service TDM/PON management [8-13]. All are impractical due to their limited capacity (maximum of a few dozen of customers). For instance, a discrete Bragg grating at a unique wavelength could be placed at each DDF termination. At the CO side, different interrogation techniques have been proposed, including a broadband source, multi-wavelength laser and tunable laser and filters, etc. These systems are impractical for high numbers of subscribers due to the very large spectrum required, i.e., one wavelength for every network leg. Recently the monitoring of a limited capacity PON (4 customers) was demonstrated by exploiting Brillouin scattering [14]. This requires that DDFs be manufactured with different physical characteristics that generate and return different Brillouin frequencies which require extreme design effort compared to existing fiber network infrastructures.

In [6], we introduced a modified optical code division multiplexing (OCDM) scheme for centralized monitoring of the status of fiber links in a PON. It is simple and easy to implement, and capacity is determined by the code family cardinality. Our monitoring technology is able to support very high capacity networks; orders of magnitude larger than all previously proposed techniques [6]. By exploiting passive optical coding technology, no active component is placed in the field and no intelligent module is embedded inside the customer ONT. In addition, by transmitting the monitoring signals in the U band (1625-1675 nm, ITU-G.983, reserved for fiber monitoring) and separating the monitoring signals

Paper approved by W. C. Kwong, the Editor for Optical Networks of the IEEE Communications Society. Manuscript received November 12, 2008; revised March 10, 2009 and June 17, 2009.

M. M. Rad and L. A. Rusch are with the Electrical and Computer Engineering Department, Laval University, Quebec, Canada. They are also with the Center of Optics, Photonics, and Laser (COPL) (e-mail: mohammad.mansouri-rad.1@ulaval.ca, rusch@gel.ulaval.ca).

H. A. Fathallah is with the Electrical Engineering Department, College of Engineering, King Saud University, Riyadh, KSA, and is an adjunct professor with the Electrical and Computer Engineering Department, Laval University, Quebec, Canada (e-mail: hfathallah@ksu.edu.sa).

Digital Object Identifier 10.1109/TCOMM.2010.04.080503

and communication data, we achieve real-time, in-service fiber link status monitoring. Note that our technique only provides information on link status. The monitoring of data signal quality is another important issue, but outside of the scope of this paper.

In this paper, for the first time, we develop the required mathematical models to analyze a generalized OC based monitoring system. This includes the one-dimensional scheme initially introduced in [6], and the two-dimensional scheme we propose in this paper. We derive closed-form expressions for performance, including *interference probability*, and the *signal-to-interference ratio* (SIR). We address the effect of the PON geographical distribution on the system performance. For our analysis, we consider five PON distribution models. Our numerical results show that the geographical distribution has a significant impact on the SIR; this notwithstanding, uniform radial distribution (which is simple and more accessible analytically) provides a reasonable approximation for performance of all distributions considered, and can be quite tractable in analyzing systems [7]. The relative importance of detection noises and interference is not studied here; the *signal-to-noise ratio* (SNR) will be addressed in a separate study [7].

Our focus (in this paper) is on fiber fault identification in a branched network such as a PON [6]. Fault localization in a PON is another important issue which is beyond the study of this paper [1-6]. In this article, we examine only interference effects and neglect other noise sources, hence our figure of merit is the SIR.

The rest of the paper is organized as follows. In section II, we describe the one-dimensional (1D) and the two-dimensional (2D) OC monitoring system. Moreover, we provide an analysis for the power/loss budget of these monitoring systems. In section III, we mathematically model all system components and operations, including coding, decoding, and correlation assuming a linear system. We derive an expression for the detected monitoring signal that is a weighted and delayed sum of autocorrelation and cross-correlation functions. We highlight and explain important differences between standard OCDMA systems and our application. In sections IV and V, we address the effect of the PON geographical distribution on the performance of the monitoring system. We derive new closed-form approximate expressions for the SIR and study its asymptotic behavior. Finally, section VI concludes our paper.

II. OCDM Monitoring System

In Fig. 1, we illustrate the principle of our PON monitoring system [6]. We distinguish branches, that is, each distribution-drop fiber (DDF), in the PON using a specific passive optical encoder placed at the DDF end. The central office transmits an optical pulse to the network on a single waveband in the U band per the desired pattern (pulse width and pulse repetition rate). Each subpulse (at the fiber end) is separated from the data signal by a U band wavelength selector (WS) at the ONT, and then coded and reflected back to the CO by a dual function device (encoder/reflector), that we call a *coding mirror* (CM). The central office receives the sum of all the encoded monitoring signals sent back from the CMs and extracts the status information about each DDF (link) by cyclically matching the corresponding decoder to the received signal. Details of the receiver are featured in an inset in Fig. 1. Features of the autocorrelation peak could be used to asses the quality of the individual link, although in this paper we focus only on assessing status. If all the components of the network are working well, the monitoring signal (auto-correlation peak) will be strong [5]; a missing auto-correlation indicates a failure. When a break occurs in the feeder, no autocorrelation peak is observed for any DDF; the lack of a peak for all DDFs identifies the fault in feeder [6]. Given the low probability of a fiber fault, we do not address the identification of simultaneous fiber faults, other than that in the feeder (or equivalently in a fiber bundle). Recall that our technique does not provide an estimate of data signal quality, but rather fiber status.

Important differences exist between standard OCDMA and our modified version developed for fiber link status monitoring of a PON. The interference terms are only related to the monitoring channels and not the communication data. No modulation, no bit rate and no continuous transmission of data exist in our monitoring system. Instead, our system has a repetition rate that is constrained by the distance between the CO and the farthest ONTs. Repetition rates on the order of kilohertz would be typical. Contrast this with traditional data modulated OCDMA where Mb/s and Gb/s transmissions are required.

In principle, most standard OCDMA coding techniques can be applied to our monitoring technique. However, targets for encoder complexity, the considered code cardinality and interference properties of the code families, are strikingly different [15]. A wide variety of codes have been developed for coding in traditional OCDMA such as prime codes and optical orthogonal codes (OOCs). In this paper, we generalize the monitoring approach from one dimensional coding (proposed in [6]) to time$\times$wavelength (2D) coding schemes.

A. One vs. Two Dimensional Coding

A two dimensional code family is presented by a quintuplet $(F, M, w, \lambda_a, \lambda_c)$, where F is the code length, M is the number of wavelengths, w is code weight, λ_a and λ_c are maxima of the out-of-phase auto and cross correlation, respectively. We consider 1D coding as a special case of 2D coding by setting $M = 1$. Figure 1 also shows two implementations of a 2D CM. A generic 2D CM passive splitter implementation using tapped delay lines (TDLs), bandpass filters (BPFs) and passive splitters/combiners (PSCs) and/or circulator is illustrated [6],[15]. A more practical, multiple-FBG (MFBG) implementation is also illustrated. Each grating in this structure reflects a different wavelength in a specific time (i.e., discrete position), corresponding to a preset 2D code. Note that the FBG implementation obviates U band WS at the DDF ends, as well as the additional circulator/coupler required for the PSC based scheme, hence reducing the component count and the total CM loss.

For 1D coding, in Fig. 1, no BPF is required and all the gratings reflect the same center wavelength and each FBG

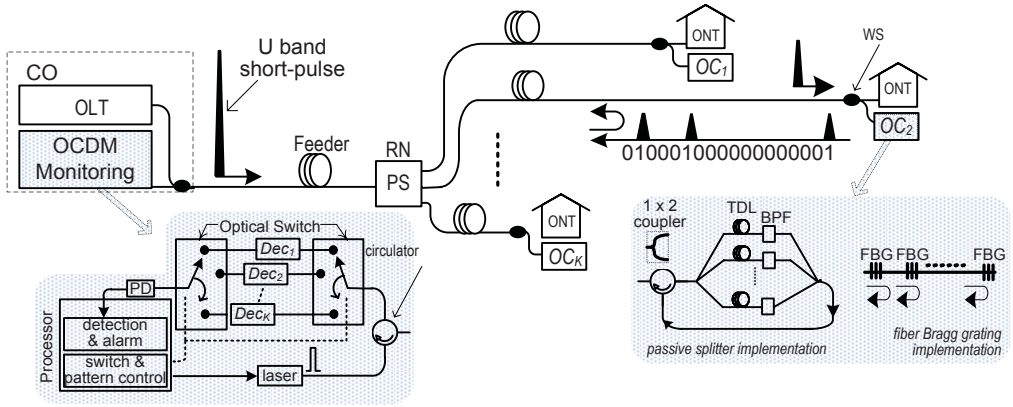

Fig. 1. Principle of operation of OC monitoring, including 2D implementation schemes for coding mirrors. The same implementation is considered for encoding/decoding operation.

must have relatively low and distinct reflectivity in order for the reflected pulses to have equal amplitudes and to reduce internal reflections among gratings; this imposes fabrication constraints [16]. Note that the single gratings for 2D coding are tuned to reflect different wavelengths, while those for 1D coding all reflect the same wavelength.

B. Power/Loss Budget

The monitoring signal travels the complete optical network round trip; hence it exhibits a loss that is much higher than that of the data which travels in only one direction. Figure 2 illustrates the power/loss budget taking into account all network elements downstream and upstream. The near-horizontal lines in the power/loss budget curve in Fig. 2 correspond to fiber attenuation in the feeder and DDFs. Recall that fiber loss in the U band for monitoring signals is higher than in the data band. The vertical lines correspond to abrupt losses due to the RN passive splitter/combiner in downstream/upstream, the encoder (CM at the DDF's end), and the decoder (at the CO). Significant loss is incurred by the encoder/decoder and the RN splitter/combiner. The RN related loss depends directly on the number of customers (capacity) and cannot be reduced. The encoder/decoder loss depends on the implementation used, i.e., CMs loss can be optimized. For example, a GPON with 128 customers has a RN with 21 dB splitting loss for upstream and down-stream, i.e., total loss of 42 dB. A 1D FBG CM with 25% reflectivity (code weight four, i.e., $w = 4$) introduces an insertion loss of 6 dB for each coding and decoding operation. A 2D FBG CM with 100% reflectivity theoretically introduces no insertion loss, hence saving 12 dB in the loss budget compared to the 1D setting. Recall that no WS, circulator or additional coupler (as illustrated in Fig.1) is required for a FBG based scheme.

The PSC implementation of Fig. 1, has much higher CM insertion loss than the FBG implementation. For example, a PSC CM with four branches ($w = 4$) induces a minimum of 12 dB loss due to splitting and combining. An additional coupler (circulator) increases the loss budget 3 dB (2 dB), resulting in a total loss of 15 dB (14 dB) for the PSC CM scheme; in this scheme the CM loss is higher than the decoder loss in the OCDM monitoring recevier. Figure 2 plots losses as various elements of the network are encountered (i.e., vs.

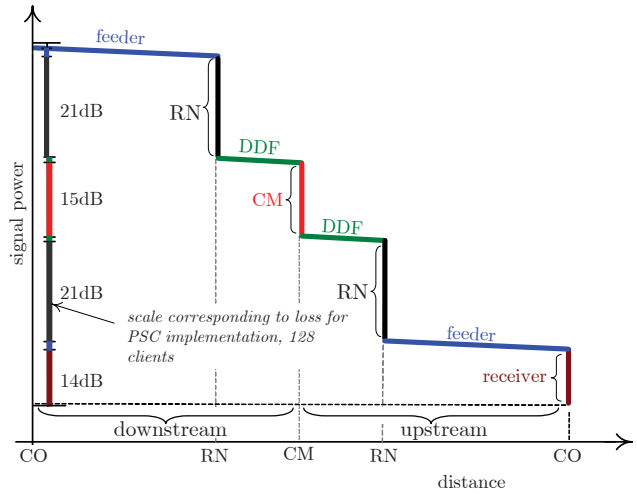

Fig. 2. Power/loss budget map of OC monitoring pulse. The example is illustrated for a GPON with 128 branches, and PSC encoder/decoder implementation of Fig. 1.

distance). The signal power scale provided is for the specific case of a 128 GPON using the PSC implementation. The 2 dB circulator loss at the CO is considered as a part of the receiver. Note that the decoders at the CO, do not need an additional circulator/coupler.

The cumulative encoding-decoding attenuation in the field domain ($\alpha_e \times \alpha_d$) is experienced by every monitoring pulse sent from the CO. Our system performance depends on the height of the autocorrelation peak, the sum of w pulses. Therefore, the useful power for decision at the receiver (in Fig. 1) is proportional to $x_{aut} \triangleq w\alpha_e^2\alpha_d^2$, i.e., the peak depends on the code weight and the coding/decoding implementation (PSC or FBG). For an FBG based 2D CM of Fig. 1, 100% reflectivity is a reasonable assumption. For an FBG based 1D CM, the best achievable reflectivity is the inverse of the code weight [16]. Recall that commercial versions of PSC are only available in powers of two. Let $w_0 \triangleq \lceil \log_2 w \rceil$ where $\lceil \cdot \rceil$ denotes the smallest integer greater than its argument. The PSC splitting loss is $\frac{1}{w_0}$; we neglect insertion loss of the BPFs and the optical switches and assume the same implementations for both encoder and decoder in Fig. 1. Therefore, we can

express $x_{aut} \triangleq 10\log_{10}\left(w\alpha_e^2\alpha_d^2\right)$ in dB as

$$-\begin{cases} 40\log w_0 - 10\log w + 2 & \text{PSC + circulator} \\ 40\log w_0 - 10\log w + 6 & \text{PSC + 1:2 coupler} \\ 10\log w & \text{1D - FBG} \\ 0 & \text{2D - FBG} \end{cases} \quad (1)$$

Clearly x_{aut} for the PSC structure is minimized when the code weight is a power of two, i.e., $w_0 = w = 2, 4, 8$, etc. For a FBG based implementation for the 1D coding scheme, x_{aut} is an increasing function of the code weight; as the code weight increases x_{aut} decreases, degrading performance. For a 2D FBG scheme, there is no encoding/decoding loss ($x_{aut} = 1$). We should maximize x_{aut} to minimize the total encoding/decoding loss ($\alpha_e^2\alpha_d^2$) and component count, while providing a good auto-correlation peak vs. the cross-correlation spikes (w vs. λ_c). As a trade-off, in our numerical simulation, we use $w = 4$ and consider a unitary cross correlation code family, i.e., $\lambda_c = 1$. To facilitate the synchronization process, we limit the auto-correlation side lobes to one, i.e., $\lambda_a = 1$ [15].

An FBG based implementation shows a clear advantage, compared to PSC based structures, in terms of simplicity, component count, and power/loss budget given by (1). The loss budget advantage results in superior performance (in terms of SNR) of an FBG based implementations with respect to PSC based structures. This issue is to be investigated in future work [7].

III. System Model

A. Encoding/Decoding

We start with a 2D CM model, and will consider the 1D CM as a particular case of the 2D model. Assuming a linear operation, the electrical field impulse response of the 2D CM for client number k, can be expressed as

$$e_k(t,\lambda) = \sum_{j=1}^{w} \alpha_e \delta\left(t - \tau_{k,j}, \lambda_{k,j}\right) \quad (2)$$

where α_e denotes the total encoder attenuation in the field domain (assumed identical for each of the w reflected pulses), $\tau_{k,j}$ and $\lambda_{k,j}$ are respectively the delay and center wavelength of the j^{th} reflected pulse, and δ is the Dirac delta function.

The decoder function $d_k(t,\lambda)$ with insertion loss of α_d is similar to that of the encoder; the delay term $\tau_{k,j}$ is replaced by $T - \tau_{k,j}$, giving autocorrelation peak at the interval $[T - T_c, T]$ where T_c is the transmitted pulse duration and T is the repetition interval. The 1D CM model can be derived from equation (2) by assuming the same center wavelength for all optical pulses, i.e., $\lambda_{k,j} = \lambda_0$.

Let $a_k(t,\lambda)$ be the autocorrelation function, defined as the convolution of the k^{th} encoder with its decoder, $k \in \{1, 2, ..., K\}$; let $c_{k,m}(t,\lambda)$ be the cross-correlation function defined as the convolution of the k^{th} encoder (e_k) with the m^{th} decoder (d_m), $k \neq m$. With these definitions,

$$a_k(t,\lambda) \triangleq e_k(t,\lambda) \otimes d_k(t,\lambda) \quad (3)$$

$$c_{k,m}(t,\lambda) \triangleq e_k(t,\lambda) \otimes d_m(t,\lambda) \quad (4)$$

where $\otimes$ denotes the convolution operation.

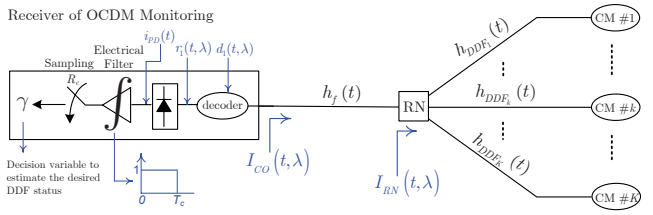

Fig. 3. Impulse response definitions of different system segments in the monitoring channel.

B. Network Impulse Responce

As shown in Fig. 3, the total (roundtrip) impulse response of the network observed from the RN, $I_{RN}(t,\lambda)$, is

$$I_{RN}(t,\lambda) = \frac{1}{K}\sum_{k=1}^{K} \xi_k h_{DDF_k}(t) \otimes e_k(t,\lambda) \otimes h_{DDF_k}(t) \quad (5)$$

where $h_{DDF_k}(t)$ and $\xi_k \in \{0,1\}$ are the impulse response and the health status of DDF_k, $k = 1, .., K$, respectively. When DDF_k is healthy (i.e., $\xi_k = 1$) it participates in the RN impulse response in (5); when DDF_k is broken (i.e., $\xi_k = 0$), the transmitted pulse is neither encoded nor reflected. In Section IV, we explain how the interference statistics in our system depends on DDF health status ξ_k. The factor $\frac{1}{K}$ shows the total attenuation in the field domain due to PSC in upstream and downstream paths at the RN. Let $h_f(t)$ be the impulse response of the feeder, and assume forward and backward impulse responses are identical (i.e., neglecting asymmetric fusions and connections). The total signal returning to the CO, $s(t,\lambda)$, can be written as

$$\begin{aligned} s(t,\lambda) &= \Pi(t,\lambda) \otimes I_{CO}(t,\lambda) \\ &= \Pi(t,\lambda) \otimes h_f(t) \otimes I_{RN}(t,\lambda) \otimes h_f(t) \end{aligned} \quad (6)$$

where $\Pi(t,\lambda)$ denotes the transmitted pulse with (chip) duration T_c, and $I_{CO}(t,\lambda)$ is the network impulse response from the CO point of view as in Fig.3. For both 1D and 2D coding schemes, $\Pi(t,\lambda)$ can be a laser pulse (a comb of lasers for 2D) and/or a broadband source (BBS) pulse [7].

C. Optical Decoded Signal

Depending on the DDF being monitored, the received signal passes through the appropriate decoder in Fig.1. We assume that we monitor the first DDF corresponding to encoder-decoder pair number 1 and take the index $k \in \{2, ..., K\}$ to refer to the interfering signal from client k. The decoded optical signal is $r_1(t,\lambda) = A_1(t,\lambda) + \sum_{k=2}^{K} B_{1,k}(t,\lambda)$; where the first term is the desired signal and the second term is the undesired interference, i.e.,

$$\begin{aligned} A_1(t,\lambda) \triangleq \frac{1}{K} &\underbrace{h_f(t) \otimes h_{DDF_1}(t)}_{forward\ path} \\ &\otimes \tilde{a}_1(t,\lambda) \otimes \underbrace{h_{DDF_1}(t) \otimes h_f(t)}_{backward\ path} \end{aligned} \quad (7)$$

$$B_{1,k}(t,\lambda) \triangleq \frac{1}{K} h_f(t) \otimes h_{DDF_k}(t) \otimes \tilde{c}_{1,k}(t,\lambda) \otimes h_{DDF_k}(t) \otimes h_f(t) \quad (8)$$

where $\tilde{a}_1(t,\lambda) \triangleq a_1(t,\lambda) \otimes \Pi(t,\lambda)$ and $\tilde{c}_{1,k}(t,\lambda) \triangleq c_{1,k}(t,\lambda) \otimes \Pi(t,\lambda)$ denote the pulse shape after encoding and decoding for client 1 and client k, respectively. We use a delay and attenuation model for the feeder and DDFs, i.e., $h_f(t) = e^{-\alpha_a l_f/2}\delta(t - 2\frac{l_f}{c})$ and $h_{DDF_k}(t) = e^{-\alpha_a l_{DDF_k}/2}\delta(t - 2\frac{l_{DDF_k}}{c})$ where c is the speed of light in the fiber and α_a is attenuation factor of fiber in neper/meter in the monitoring U band; l_f is the length of the feeder, while l_{DDF_k} is the length of the k^{th} DDF. This yields

$$B_{1,k}(t,\lambda) = \frac{1}{K} e^{-\alpha_a l_k} \tilde{c}_{1,k}\left(t - 2\frac{l_k}{c}, \lambda\right) \quad (9)$$

where $l_k \triangleq l_f + l_{DDF_k}$ is the distance from the CO to the k^{th} client. Using (2)-(4) in conjunction with (7)-(10) we obtain

$$A_1(t,\lambda) = \alpha_L \frac{\alpha_e \alpha_d e^{-\alpha_a l_1}}{K} \sum_{u=1}^{w} \Pi\left(t - (T - T_c + 2l_1/c), \lambda_{1,u}\right) \quad (10)$$

where detection takes place during $t \in T_{obs}$ an observation window of length T_c around the arrival of the desired pulses return, i.e., $T_{obs} = \left(T - T_c + 2\frac{l_1}{c}, T + 2\frac{l_1}{c}\right)$. The factor α_L is included to account for other attenuations in the system such as the circulator at the CO, splicing, connectors, etc. Note that the autocorrelation peak of $A(t,\lambda)$ consists of w subpulses. The cross-correlation term $B_{1,k}(t,\lambda)$ reduces to the equation shown in the top of the next page.

where we have assumed the worst-case "chip synchronous", i.e., subpulses arriving within one pulse width, T_c, of each other provide as much interference as two subpulses arriving simultaneously. Subpulses outside the observation window do not have any effect; hence the restriction in the summation $T_c \geq \left|2\frac{l_1 - l_k}{c} + \tau_{1,u} - \tau_{k,v}\right|$. As we consider only unitary cross-correlation codes ($\lambda_c = 1$), the double summation contains at most one non-zero term for each interfering user k, i.e., at most $K-1$ non-zero terms.

IV. Customer Geographic Distribution

A. Correlation Distance

The pulse repetition interval must be greater than the maximum round-trip time in the network. The detection of the autocorrelation peak occurs during a window of width T_c. Subpulses coming from a CM_1 located sufficiently distant from the desired CM_1 (i.e., $l_k \gg l_1$) will not contribute to the interference, as illustrated in Fig.4, as they arrive outside the observation interval T_{obs}. How far must a potential interferer be from the desired user to not contribute to the interference?

An initial pulse of duration T_c generates w subpulses appearing somewhere in an interval FT_c wide. After decoding, the autocorrelation signal covers an interval $(2F-1)T_c$ wide, see Fig. 4. Interference arriving in the first half of the autocorrelation may overlap with the peak and impact detection. The delay of an interferer relative to the start of the autocorrelation is twice (due to roundtrip travel) the difference

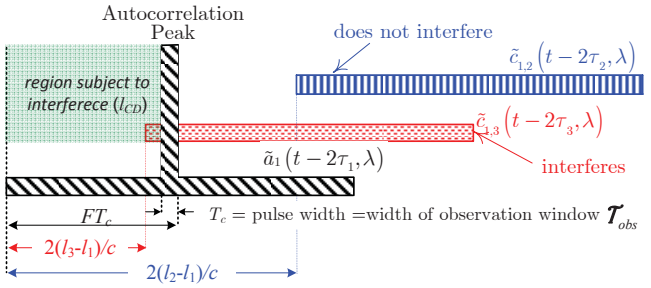

Fig. 4. Optical decoded signal: illustration of the interference conditions for autocorrelation function $\tilde{a}_1(t-2\tau_1,\lambda)$ and two cross-correlation functions; note client 2 does not generate interference, while client 3 does.

of their distances, divided by the speed of light. We define the *correlation distance*, l_{CD}, as the relative distance between two clients after which their CM sequences cannot interfere with each other. Thus only clients with

$$|l_1 - l_k| \leq l_{CD} \triangleq cFT_c/2 \quad (12)$$

can contribute to interference.

B. Interference Criteria and Probability

We have seen several criteria that establish if subpulses from CM_k contribute to the decoded signal. First, the link must be healthy, i.e., without a fiber break in the k^{th} branch. The binary random variable ξ_k equals zero when the link is broken. For our analysis we assume $\{\xi_k\}$ are independent, identically distributed (i.i.d.) Bernoulli random variables with fault probability $\Pr(\xi_k = 0) = p_\xi$. For our monitoring system we have $p_\xi \ll 1$, as is the case in practical systems.

The second criterion is that CM_k be located within the correlation distance of the desired user. Let the binary random variable $\zeta_k = 1$ indicate that CM_k is located within the correlation distance of the desired CM_1. We assume $\{\zeta_k\}_{k=2}^{K}$ are i.i.d., as all users are randomly located in the service area.

Finally, let θ_k be the binary random variable that indicates CM_k has nonzero cross-correlation with the desired signal. We have $\theta_k = 1$ when there exists (u,v) such that the position and wavelength $(\tau_{1,u}, \lambda_{1,u})$ of the u^{th} subpulse in code one coincides with that of the v^{th} subpulse in code k $(\tau_{k,v}, \lambda_{k,v})$. As we consider only unitary cross-correlation codes ($\lambda_c = 1$), so at most one such pair (u,v) exists. This criterion can be written as $T_c \geq \left|2\frac{l_1 - l_k}{c} + \tau_{1,u} - \tau_{k,v}\right|$ and $\lambda_{1,u} = \lambda_{k,v}$. Let υ_k be the coincident wavelength $\upsilon_k \triangleq \lambda_{1,u} = \lambda_{k,\upsilon_k}$. Due to the duration of the coded pulse sequence, coincidence can only occur when $|l_1 - l_k| \leq l_{CD}$. The greater the difference between l_1 and l_k, even if smaller than the correlation distance, the less likely $\theta_k = 1$. We can upper bound $\Pr(\theta_k = 1)$ by assuming the worst case, i.e., $l_1 = l_k$. Therefore we define the binary random variable $\tilde{\theta}_k$ that is one when $|\tau_{1,u} - \tau_{k,v}| \leq T_c$ and $\lambda_{1,u} = \lambda_{k,v}$. Note that l_1 and l_k no longer appear, so $\tilde{\theta}_k$ are independent of $\underline{l} = [l_1, l_2, ..., l_K]$, the vector of fiber lengths. Thus, $\tilde{\theta}_k$ is the traditional "hit" in OCDMA data communications. For a random choice of interfering client, the probability that that client will have a coincident pulse with client one, for the family of $(F, M, w, \lambda_a = \lambda_c = 1)$, is $\Pr\left(\tilde{\theta}_k = 1\right) \cong \frac{w^2}{MF}$ [15].

$$B_{1,k}(t,\lambda) = \alpha_L \frac{\alpha_e \alpha_d e^{-\alpha_a l_k}}{K} \sum\sum_{\left\{(u,v) \,\middle|\, \substack{\lambda_{1,u}=\lambda_{k,v} \text{and} \\ T_c \geq |2(l_1-l_k)/c+\tau_{1,u}-\tau_{k,v}|}\right\}} \Pi\left(t - T - \tau_{1,u} + T_c - 2\frac{l_1}{c}, \lambda_{1,u}\right) \tag{11}$$

Finally, we can say that CM_k contributes to the total interference when all three independent interference criteria hold, that is, $\rho_k \triangleq \xi_k \cdot \theta_k \cdot \zeta_k = 1$. The probability of this event can be upper bounded by $\Pr(\xi_k \cdot \theta_k \cdot \zeta_k = 1) \leq \Pr\left(\xi_k \cdot \tilde{\theta}_k \cdot \zeta_k = 1\right)$ so that

$$\begin{aligned} \Pr(\rho_k = 1) &\leq \Pr(\xi_k = 1)\Pr(\widetilde{\theta} = 1)\Pr(\zeta_k = 1) \\ &= (1-p_\xi)\tfrac{w^2}{MF} \times \begin{cases} 1 & |l_k - l_1| \leq \ell_{CD} \\ 0 & otherwise \end{cases} \end{aligned} \tag{13}$$

Note $(1-p_\xi)\frac{w^2}{MF}$ is an upper bound on the hit probability.

C. Decoded Signal

By exploiting our interference criteria and the choice of unitary cross-correlation codes we have $r_1(t,\lambda,\underline{l})$ given by

$$\frac{\alpha_e \alpha_d}{K} \alpha_L \left[e^{-\alpha_a l_1} \xi_1 \sum_{u=1}^{w} \Pi(t, \lambda_{1,u}) + \sum_{k=2}^{K} \rho_k e^{-\alpha_a l_k} \Pi(t, \lambda_{k,v_k}) \right] \tag{14}$$

during the observation window T_{obs} in the filed domain.[1] Recall that $r_1(t,\lambda,\underline{l})$ refers to the decoded optical signal in the field domain; the decision statistic is derived from the photo-detected signal whose current is proportional to equation (15) given at the top of the next page.

In this paper we consider only interference and (16) neglects detection noises and coherence effects. These noises are addressed in [7]. We integrate (16) over the observation interval T_{obs} to find the decision statistic. As the leading multiplicative factor in (16) is the same for both the desired user and the interference, it will cancel out in the signal-to-interference ratio and need not be retained in our analysis. Therefore the decision statistic γ (in Fig.3) can be written as

$$\gamma = \xi_1 w e^{-2\alpha_a l_1} + \sum_{k=2}^{K} \rho_k e^{-2\alpha_a l_k} \tag{16}$$

We next focus on the statistics of ρ_k assuming various random geographical distributions for the CMs.

D. Client Distribution

In general, PON provides services to both residential and business users [17]. Residential users occupy multi-dwelling units (MDU) and single-family-dwelling units (SFWU). Business users occupy multi-tenanted units (MTU) such as office blocks or towers and single tenanted units (STU) such as stand-alone office building or warehouses.

The PON deployment depends highly on the geography of the clients in the network [17,18]. For instance, the MDU PON topology is considered as the most likely deployment model in Europe and in Asia. In this case, a good statistical model for deployment of ONTs is a uniform distribution along a corridor on each floor. The distribution of the users also depends on the proximity of the RN, for example one RN per floor or one RN per building. In North America more than 80% of the users are independent units (SFWU), thus more dispersed geographically. Clearly, the geographical distribution of the users can vary from installation to installation and depends on a variety of parameters. To our knowledge there is no explicit study on the geographical distribution of the users in a PON. In [18] the authors show via simulation that the distribution of the households changes as the topology and the deployment technology changes. In this paper, we consider five geographical models namely uniform area and our new proposed uniform radial distributions, which match well those presented in [18]. We will show the uniform radial distribution, while simple and easy to model, provides a reasonable approximation for the system performance of all other distributions considered.

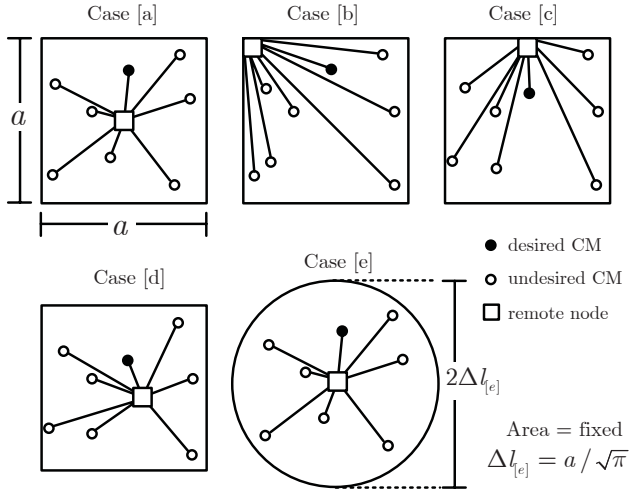

Fig. 5. PON costumer geographical distributions for fixed coverage area and fixed number of users: $[a]$-$[d]$ uniform area distributions and $[e]$ uniform radial (UR) distribution.

We first consider a uniform area distribution of the client locations over a square coverage region with four positions for the remote node (RN): $[a]$ RN at center, $[b]$ RN at corner, $[c]$ RN at mid-boundary, and $[d]$ RN randomly placed [19]. Fig.5 illustrates these cases. Note that in all cases the coverage region has area equal a^2. Consequently, the maximum relative distance between the RN and CMs, i.e., maximum separation length is $\Delta l_{[a]} = a/\sqrt{2}$, $\Delta l_{[b]} = a\sqrt{2}$, $\Delta l_{[c]} = a\sqrt{5}/2$, and $\Delta l_{[d]} = a\sqrt{2}$. These cases are similar to distributions presented in Fig. 3 in [18]. We also consider case $[e]$, a circular coverage region with the RN located at the center. CMs in case $[e]$ have radial distance from the RN uniformly distributed over $(0, a/\sqrt{\pi})$. The maximum separation length in this case is $\Delta l_{[e]} = a/\sqrt{\pi}$, and the area is again a^2. Note that while all cases cover the same area, they have different probability

[1]The synchronization to the observation interval is an important issue, but outside the scope of this paper.

$$i_{PD}(t) = \frac{\alpha_e^2\alpha_d^2}{K^2}\alpha_L^2\left[\sum_{u=1}^{w}\xi_1\left|e^{-\alpha_a l_1}\Pi(t,\lambda_{1,u})\right|^2+\sum_{k=2}^{K}\rho_k\left|e^{-\alpha_a l_k}\Pi(t,\lambda_{k,v_k})\right|^2\right]$$
$$= \frac{\alpha_e^2\alpha_d^2}{K^2}\alpha_L^2\left|\Pi(t,\lambda)\right|^2\left[\sum_{u=1}^{w}\xi_1 e^{-2\alpha_a l_1}+\sum_{k=2}^{K}\rho_k e^{-2\alpha_a l_k}\right] \quad (15)$$

density functions (PDFs) and different maximum separation lengths with ordering $\Delta l_{[e]} < \Delta l_{[a]} < \Delta l_{[c]} < \Delta l_{[b]} = \Delta l_{[d]}$. In the next section, we see how the PDF and maximum separation length affect our monitoring system performance.

V. Signal-To-Interference-Ratio Analysis

As explained, multiple access interference (MAI) defined as the interference coming from undesired monitoring signal returns, is directly related to the geographical distribution of customers. Since in traditional OCDMA users transmit long streams of data, the interference always exists, hence degrading the signal-to-interference ratio (SIR). However in our system, the SIR is higher, as pulses have low repetition rates, allowing some CM returns to fall outside the observation window. We define SIR as the ratio of the desired signal power to the power of the interference,

$$SIR \triangleq \left[\frac{E\left\{\xi_1 w e^{-2\alpha_a l_1}\right\}}{E\left\{\sum_{k=2}^{K}\rho_k e^{-2\alpha_a l_k}\right\}}\right]^2 \quad (17)$$

where expectation is taken over the geographical distribution of $\underline{l}$, and the health status $\{\xi_k\}$. SIR is our metric for monitoring performance.

A. SIR Lower Bound

Using our definition of $\{\rho_k\}$, we can upper bound the interference power in the denominator of (18) by replacing θ_k with $\tilde{\theta}_k$. By eliminating the sum and taking $k = 2$ arbitrarily and using (13) we get the following lower bound given in (19) on the SIR.

To evaluate the conditional expectation in (19), let $p(l_k)$ be the PDF of l_k, and assume l_k are i.i.d; the PDF is nonzero over $(l_f, l_f + \Delta l_{[\ ]})$ where the maximum separation $\Delta l_{[\ ]}$ varies with geographical distribution per section IV.D, and empty brackets are to contain the index of the geographical distributions (a,b,c,d,e). For the conditional expectation, only ζ_2 depends on l_1. The impact of ζ_2 in the denominator is to modify the limits of the integration in the expectation: ζ_2 is zero everywhere except an interval with $|l_1 - l_2| \le l_{CD}$, see (13). The SIR is then lower bounded as given by (19). This lower bound is calculated numerically for each geographical distribution in our simulations.

B. Asymptotic Behavior of SIR Lower Bound for Uniform Radial PDF

For a uniform radial (UR) distribution the PDF takes non-zero values of $p(z) = \frac{1}{\Delta l_{[e]}}$ only for $z \in [0, \Delta l_{[e]}]$ where z denotes the DDF differential length, i.e., $l_k = z + l_f$. A closed form, albeit complicated, solution to the integral of (19) can be found. The SIR has three regions of definition

$$\begin{array}{l} SIR_{UR}\left(l_{CD} > \Delta l_{[e]}\right) \\ SIR_{UR}\left(\Delta l_{[e]} > l_{CD} > \Delta l_{[e]}/2\right) \\ SIR_{UR}\left(\Delta l_{[e]}/2 > l_{CD} > 0\right) \end{array} \quad (20)$$

The main difference among these regions is the relative importance of the interferers. We will content ourselves with the asymptotic behavior of the SIR lower bound. For the SIR lower bound in the regions defined in (20) we evaluated the closed form solutions only for two PON extremes, i.e., low and high density PONs. A family of multi-wavelength OOC with $(F = Kw(w-1), M, w, \lambda_a = \lambda_c = 1)$ is considered for our analysis. The required code length F is calculated by using the Johnson bound for 1D OOCs with cardinality of K (network size) [15]. To save space we only report the results.

i) High-Density PON: A large number of customers (i.e., $K \gg 1$) located in a small zone (i.e., small $\Delta l_{[e]}$), requires large code lengths (i.e., $F \gg 1$). This results in a large correlation distance (i.e., $l_{CD} \ge \Delta l_{[e]}$ or the first region in (20)). The SIR_{UR} in this situation corresponds to

$$SIR_{UR} = [M(w-1)]^2 \quad \text{for} \quad l_{CD} \ge \Delta l_{[e]} \quad (21)$$

Note that this situation can also occur for long transmitted pulses, i.e., larger T_c. Increasing T_c proportionally increases the correlation distance and so $l_{CD} \ge \Delta l_{[e]}$ is more likely.

ii) Low-Density PON: For a low density PON, that is when clients are sparse, the correlation distance is much smaller than the customer's distribution length in the network (i.e., $l_{CD} \ll \Delta l_{[e]}$, the third region in (20)). Under this condition the SIR_{UR} is approximated by

$$SIR_{UR} = \left[\frac{M(w-1)\Delta l_{[e]}}{2 l_{CD}}\right]^2 \quad \text{for} \quad l_{CD} \ll \Delta l_{[e]} \quad (22)$$

Again note that this situation can occur for both very low network sizes, i.e., K very small, or very short pulse width T_c. In both (21) and (22) we observe the factor M that corresponds to the number of available wavelengths in the coding system. For 1D scheme $M = 1$.

In the worst case scenario when the maximum relative distance between CMs, i.e., maximum separation length, is much smaller than CD, i.e., $\Delta l_{[e]} \ll l_{CD}$, all CMs are close enough to interfere with the desired one. In this case the SIR is similar to traditional OCDMA systems, i.e., the situation described by (21). On the other hand, when $l_{CD} \ll \Delta l_{[e]}$, only very close CMs are able to interfere with the desired one. Note that in this situation the SIR is proportional to the

$$\sqrt{SIR} \geq \frac{w\,(1-p_\xi)\,E\left\{e^{-2\alpha_a l_1}\right\}}{\sum_{k=2}^{K} E\left\{\xi_k \cdot \tilde{\theta}_k \cdot \zeta_k \cdot e^{-2\alpha_a l_k}\right\}} = \frac{MF \cdot E\left\{e^{-2\alpha_a l_1}\right\}}{w(K-1)E\left\{\zeta_2 \cdot e^{-2\alpha_a l_2}\right\}} = \frac{MF \cdot E\left\{e^{-2\alpha_a l_1}\right\}}{w(K-1)E_{l_1}\left\{E_{l_2|l_1}\left\{e^{-2\alpha_a l_2}\zeta_2|\, l_1\right\}\right\}} \tag{18}$$

$$\sqrt{SIR} \geq \frac{MF \cdot \int p(l_1) e^{-2\alpha_a l_1} dl_1}{w(K-1)\int p(l_1)\left[\int_{\max(l_f, l_1 - l_{CD})}^{\min(l_f+\Delta l_{[\,]}, l_1+l_{CD})} e^{-2\alpha_a l_2} p(l_2) dl_2\right] dl_1} \tag{19}$$

square of the maximum length $\Delta l_{[e]}$ and inversely proportional to the square of the correlation distance l_{CD}, see (22).

C. Numerical Results

We observe from the expressions developed previously that the SIR depends on many parameters that could be grouped in three sets $S_1 = \{K, \Delta l_{[\cdot]}, PDF\}$, $S_2 = \{CF\}$, and $S_3 = \{T_c\}$, where CF refers to the selected code family and PDF is the geographical distribution of clients. The elements of S_1 are related to the physical, geographical parameters of the PON: the number of clients (K), the farthest client served by the network ($\Delta l_{[\cdot]}$), and the clients distribution (PDF). S_2 is related to the code design including: code family, code weight, length and number of wavelengths as well as the correlation properties. Elements of S_2 are interdependent and their values are subject to the design constraints imposed by S_1 and system requirements. We consider the pulse duration T_c in a separate set because it is independent of all other parameters.

In Fig.6, we present the SIR versus the network capacity K for both coding types 1D and 2D and for all the five geographical distributions $[a]$ to $[e]$ using numerical techniques to calculate (19) by considering a code family with $(F = Kw(w-1)+1, M = w, w = 4, \lambda_a = \lambda_c = 1)$ and setting the pulse duration to $T_c = 1$ns. In Fig.6, plots on the left (respectively right) report results for 1D codes (respectively 2D). Upper plots (respectively lower) have coverage area of 0.25 km^2 (respectively 5 km^2). We observe that the SIR curves of the five cases $[a]$-$[e]$ approach (or converge to) the same asymptote for large network sizes and deviate for low network sizes; this observation applies to both 1D and 2D codes. It is obvious that the 2D scheme performs better than the 1D due to additional gain in the wavelength dimension, i.e., M (here equal to 4). In both 1D and 2D cases, as the coverage area increases, SIR increases due to degradation of the average interference.

From Fig.6, we clearly observe $SIR_{[a]} \leq SIR_{[e]} < SIR_{[c]} \approx SIR_{[d]} < SIR_{[b]}$. This does not follow the order of maximum separation lengths for the different geographical distribution as mentioned in section IV.D. This illustrates that $\Delta l_{[\cdot]}$ is not sufficient to deduce relative SIR; the form of the PDF plays a key role in the SIR, i.e., the interference depends on both PDF and $\Delta l_{[\cdot]}$. Consequently, for small

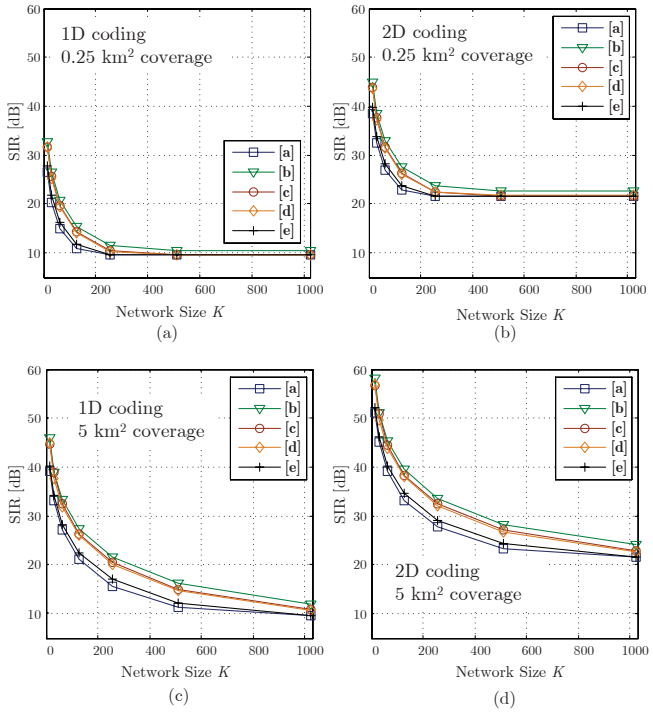

Fig. 6. SIR lower bound for five geographical distributions vs. number of clients supported K: 1D scheme (first column), 2D scheme (second column) coverage area 0.25 km^2 (first row) and 5 km^2 (second row).

network capacities, the maximum deviation in SIR is around 6 dB. Recall that in each subplot of Fig.6, the pulse width and coverage area are fixed. Therefore, this deviation comes from the difference in the geographical distributions (both the PDF and $\Delta l_{[\cdot]}$). For a fixed pulse width T_c and network size K (i.e., fixed correlation distance l_{CD}), the probability that two clients are located closer than l_{CD} has the smallest (largest) value for case $[b]$ (case $[a]$). Hence, case $[a]$ (case $[b]$) provides the smallest (highest) SIR. The UR model (SIR_{UR}, case $[e]$) shows intermediate performance compared to the worst and best cases $[a]$ and $[b]$ respectively. The SIR_{UR} could be then used as an approximation of any geographical distribution with a maximum of 6 dB deviation from results for other distributions. For K large, the PDF has little impact on the SIR.

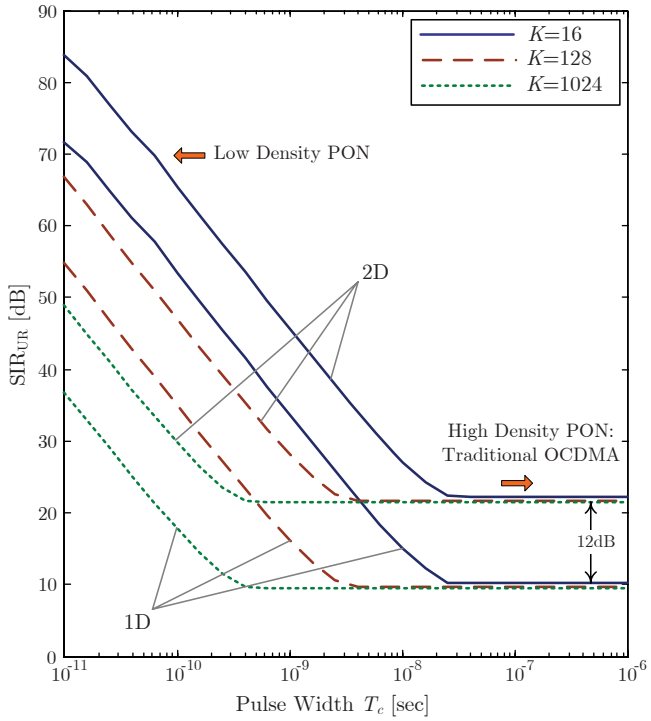

Fig. 7. SIR vs. transmitted pulse duration for uniform radial distribution and 1 km^2 coverage area; 1D and 2D coding schemes.

D. SIR vs. Pulse Duration T_c

As mentioned before, the correlation distance is proportional to the pulse duration. Reducing T_c directly reduces the CD consequently reducing the interference probability in (13). In Fig.7, we plot the SIR versus the transmitted pulse duration for both 1D and 2D schemes for a UR distribution, case $[e]$. We plot the SIR for a family of codes with $(F = Kw(w-1)+1, M = w, w = 4, \lambda_a = \lambda_c = 1)$, three different network sizes, K = 16,128 and 1024, and a coverage area of 1 km^2. From this figure, we observe three important characteristics.

Firstly, the slope of the SIR is quite independent of the network size or coding scheme, and equals -20dB/decade. This relationship can be seen in (22), the asymptotic low density PON. In dB, (22) gives $20\log_{10}\left(M(w-1)\Delta l_{[e]}/2l_{CD}\right) = C - 20\log_{10} T_c$ where C is a constant value determined by S_1 and S_2. Thus, it can be seen that SIR and pulse duration are linearly related. Next, the SIR curve reaches a floor where the correlation distance is equal to the maximum separation length (i.e., $l_{CD} = \Delta l_{[e]}$), corresponding to a pulse width of $T_c = 2\Delta l_{[e]}/cF$. This point moves with the network size as the code length F depends on the network size K. Finally, the floor corresponds to traditional OCDMA-like conditions where $l_{CD} \geq \Delta l_{[e]}$; the SIR does not depend on the pulse width. Note that reducing the pulse width normally reduces the total launched energy to the network. Monitoring system should normally use very sensitive high gain APD detectors [7].

VI. Conclusion

We analyzed the performance of optical coding (OC) PON monitoring. We developed new mathematical models for our monitoring system elements and signal processing operations. We considered the wavelength×time (two-dimensional) coding in addition to the one dimensional coding of [6]. We illustrated that the geographical distribution of the clients affects the interference in our system, by considering five geographical distributions describing realistic PON systems. We derived a closed form lower bound for signal-to-interference ratio (SIR) as the measure of our monitoring system performance. We showed that the uniform radial (UR) distribution, an analytically tractable distribution, gives accurate performance estimation for all the distributions considered. In addition, our monitoring system suffers less from interference than does traditional OCDMA. Our results show that SIR is sufficient to successfully monitor the network. We found that reducing the pulse width is a good strategy to increase the SIR. We also derived closed form expressions for the asymptotic behavior of the SIR in the case of a UR distribution. These expressions provide a reasonable predictor of SIR with other geographical distributions.

References

[1] A. Girard, "FTTx PON Technology and Testing," EXFO Electro-Optical Engineering Inc., Canada, 2005 (ISBN: 1-55342-006-3).
[2] R. Davey and D. Payne, "The future of optical transmission in access and metro networks—an operator's point of view," *European Conf. Optical Commun.* (ECOC), Paper We 2.1.3, 2005.
[3] G. Talli, C. W. Chow, E. K. MacHale, and P. D. Townsend, "High split ratio 116km reach hybrid DWDM-TDM 10Gb/s PON employing R-ONUs," *European Conf. Optical Commun.* (ECOC), Paper Mo4.5.2, 2006.
[4] F. Caviglia and V. C. Biase, "Optical maintenance in PONs," *European Conf. Optical Commun.* (ECOC), Madrid, Spain, pp. 621-625, 1998.
[5] D. C. Kilper, R. Bach, D. J. Blumenthal, D. Einstein, T. Landolsi, L. Ostar, M. Preiss, and A. E. Willner, "Optical performance monitoring," *IEEE J. Lightwave Technol.*, vol. 22, no. 1, pp. 294-304, Jan. 2004.
[6] H. Fathallah and L. A. Rusch, "Code division multiplexing for in-service out-of-band monitoring," *J. Optical Netw.*, vol. 6, no. 7, pp. 819-829, July 2007.
[7] M. M. Rad, H. Fathallah, and L. A. Rusch, "Performance analysis of fiber fault PON monitoring using optical coding: SNIR, SNR, and false-alarm probability," *IEEE. Trans. Commun.*, vol. 58, no. 4, Apr. 2010.
[8] S. Hann, J. Yoo, and C. Park, "Monitoring technique for a hybrid PS/WDM-PON by using a tunable OTDR and FBGs," *Measurement Science Technol.*, vol. 17, pp. 1070-1074, 2006.
[9] C. Yeh and S. Chi, "Optical fiber-fault surveillance for passive optical networks in S-band operation window," *Optics Express*, vol. 13, no. 14, pp. 5494-5498, July 2005.
[10] C. Chan, F. Tong, L. Chen, K. Ho, and D. Lam, "Fiber-fault identification for branched access networks using a wavelength-sweeping monitoring source," *IEEE Photonic Technol. Lett.*, vol. 11, no. 5, pp. 614-616, May 1999.
[11] N. Nakao, H. Izumita, T. Inoue, Y. Enomoto, N. Araki, and N. Tomito, "Maintenance method using 1650 nm wavelength band for optical fiber cable networks," *IEEE J. Lightwave Technol.*, vol. 19, no. 10, pp. 1513-1520, Oct. 2001.
[12] K. W. Lim, E. S. Son, K. H. Han, and Y. C. Chung, "Fault localization in WDM passive optical network by reusing down-stream light source," *IEEE Photonic Technol. Lett.*, vol. 17, no. 12, pp. 2691-2693, Dec. 2005.
[13] S. B. Park, D. K. Jung, H. S. Shin, D. J. Shin, S. Hwang, Y. Oh, and C. Shim, "Optical fault monitoring method using broad-band light source in WDM-PON," *IEE Electron. Lett.*, vol. 42, no. 4, Feb. 2006.
[14] D. Iida, N. Honda, and F. Ito, "Design of identification fibers with individually assigned Brillouin frequency shifts for monitoring passive optical networks," *IEEE J. Lightwave Technol.*, vol. 25, no. 5, pp. 1290-1297, May 2007.
[15] G. Yang and W. C. Kwong, *Prime Codes with Applications to Wireless and Optical Networks*. Artech House, 2004 (ISBN: 1-58053-073-7).
[16] H. Fathallah, L. A. Rusch, and S. LaRochelleh, "Passive optical fast frequency-hop CDMA communication system," *IEEE J. Lightwave Technol.*, vol. 17, no. 3, pp. 397-405, Mar. 1999.
[17] [Online]. Available: http://www.ftthcouncil.org/

[18] M. D. Vaughn, D. Kozichek, D. Meis, A. Boskovic, and R. Wanger, "Value of reach-and-split ratio increase in FTTH access networks," *IEEE J. Lightwave Technol.*, vol. 22, no. 11, pp. 2617-2622, Nov. 2004.

[19] O. Pirinen, "Outage analysis of ultra-wideband system in lognormal multipath fading and square cellular configurations," *EURASIP J. Wireless Commun. Netw.*, vol. 2006, pp. 1-10.

Mohammad M. Rad received his B.S.E.E. and M.S.C. both from Sharif University of Technology in 2003 and 2005, respectively. In September 2006 he joined the Department of Electrical and Computer Engineering, Center for Optics, Photonics and Lasers (COPL), Université Laval as a PhD candidate. His research interests include fiber-optic communications, long haul data transmission, multiple access networks, network monitoring and sensor networks.

Habib A. Fathallah (S'96, M'01) received the B.S.E.E degree (with Honors) from the National Engineering School of Tunis, 1994 and the M.A. and Ph.D. degrees in electrical engineering from Laval University, Qc, Canada, in 1997 and 2001, respectively. He initiated the use of Bragg gratings technology for all-optical/all-fiber coding/decoding in Optical CDMA systems. He was the founder of Access Photonic Networks (2001-2006). He is currently with Electrical Engineering Department, College of Engineering of the King Saud University (Riyadh, KSA) and adjunct professor with the Electrical and Computer Engineering Department of Laval University (Quebec, Canada). His research interests include optical communications systems and technologies, metro and access networks, Optical CDMA, PONs and long reach PONs, FTTH, Network Monitoring, and hybrid fiber wireless (FiWi) systems.

Leslie Ann Rusch (S'91-M'94-SM'00) L. A. Rusch received the B.S.E.E. (honors) degree from the California Institute of Technology, Pasadena, in 1980 and the M.A. and Ph.D. degrees in electrical engineering from Princeton University, Princeton, NJ, in 1992 and 1994, respectively. In 1994 she joined the Department of Electrical and Computer Engineering at Université Laval, Québec, QC, Canada, where she is currently a Full Professor performing research in wireless and optical communications. She spent two years as the manager of a group researching new wireless technologies at Intel Corp. from 2001 to 2002. Her research interests include optical-code-division multiple access and spectrum sliced WDM using incoherent sources for passive optical networks; semiconductor and erbium-doped optical amplifiers and their dynamics; radio over fiber; and in wireless communications, high performance, reduced complexity receivers for ultra-wide-band systems employing optical processing.